

Article

Multichannel Sensorimotor Integration with a Dexterous Artificial Hand

Moaed A. Abd¹ and Erik D. Engeberg^{1,2,3,*} 

¹ Department of Ocean and Mechanical Engineering, Florida Atlantic University, Boca Raton, FL 33431, USA; moaed.abd@googlemail.com

² Center for Complex Systems and Brain Sciences, Florida Atlantic University, Boca Raton, FL 33431, USA

³ Department of Biomedical Engineering, Florida Atlantic University, Boca Raton, FL 33431, USA

* Correspondence: eengeberg@fau.edu

Abstract: People use their hands for intricate tasks like playing musical instruments, employing myriad touch sensations to inform motor control. In contrast, current prosthetic hands lack comprehensive haptic feedback and exhibit rudimentary multitasking functionality. Limited research has explored the potential of upper limb amputees to feel, perceive, and respond to multiple channels of simultaneously activated haptic feedback to concurrently control the individual fingers of dexterous prosthetic hands. This study introduces a novel control architecture for three amputees and nine additional subjects to concurrently control individual fingers of an artificial hand using two channels of context-specific haptic feedback. Artificial neural networks (ANNs) recognize subjects' electromyogram (EMG) patterns governing the artificial hand controller. ANNs also classify the directions objects slip across tactile sensors on the robotic fingertips, which are encoded via the vibration frequency of wearable vibrotactile actuators. Subjects implement control strategies with each finger simultaneously to prevent or permit slip as desired, achieving a $94.49\% \pm 8.79\%$ overall success rate. Although no statistically significant difference exists between amputees' and non-amputees' success rates, amputees require more time to respond to simultaneous haptic feedback signals, suggesting a higher cognitive load. Nevertheless, amputees can accurately interpret multiple channels of nuanced haptic feedback to concurrently control individual robotic fingers, addressing the challenge of multitasking with dexterous prosthetic hands.



Citation: Abd, M.A.; Engeberg, E.D. Multichannel Sensorimotor Integration with a Dexterous Artificial Hand. *Robotics* **2024**, *13*, 97. <https://doi.org/10.3390/robotics13070097>

Academic Editor: Kean Aw

Received: 16 May 2024

Revised: 24 June 2024

Accepted: 26 June 2024

Published: 30 June 2024



Copyright: © 2024 by the authors. Licensee MDPI, Basel, Switzerland. This article is an open access article distributed under the terms and conditions of the Creative Commons Attribution (CC BY) license (<https://creativecommons.org/licenses/by/4.0/>).

Keywords: prosthetic hand; robotic hand; haptic feedback; amputee; dexterous hand; electromyogram

1. Introduction

The capacity for dexterous control of a prosthetic hand and the sensation of touch are inherently intertwined [1]. Unfortunately, the potential for amputees to engage in sophisticated activities like playing sports or musical instruments remains elusive because current clinical practice with prosthetic hands affords limited control capabilities, with minimal or no awareness of corresponding fingertip touch sensations. The mastery of dexterous tasks requires both the capacity for simultaneous and individual finger control along with refined touch sensations, such as awareness of the direction that fingers are sliding [2] along the strings of a violin [3], for example (Figure 1). Although this level of control mastery remains largely in the future for amputees, it provides an ambitious goal.

With their natural hands, people can rapidly determine which direction a force is applied to their fingertips by the relative timing of ensembles of action potentials from populations of mechanoreceptors [4]. This information, along with other details like the perceived friction of the grasped object, are used to prevent grasped object slip [5] by controlling the applied grip force in nuanced ways that can vary based on the direction that disturbance forces are applied [6]. When slip does occur, neurons in the primary somatosensory cortex respond with firing rates that are related to the speed of slip or the texture of the object, and grip force compensation to prevent slip can occur reflexively or

voluntarily [3]. Recreating this level of functionality with a dexterous prosthetic hand poses a daunting challenge because it necessitates properly interpreting the intention of the user, advanced tactile sensors on the prosthesis, and a sophisticated method for haptic feedback to the user [7].

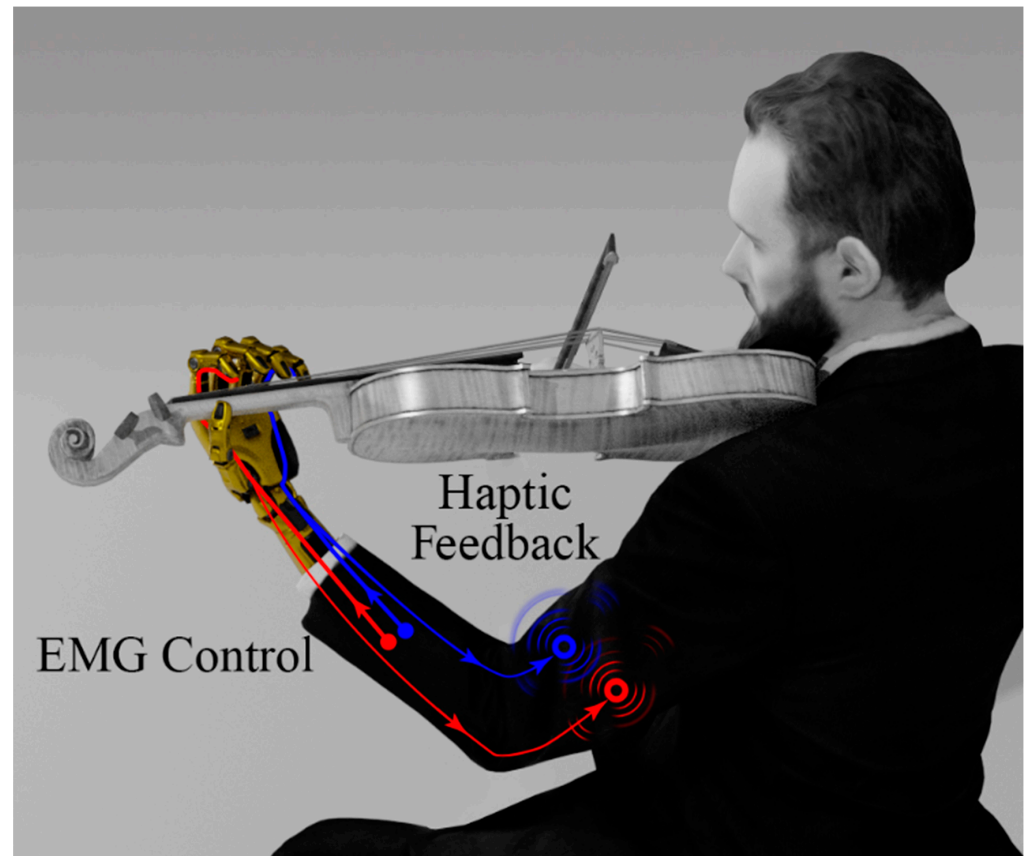


Figure 1. Complex activities such as playing a musical instrument present a great challenge to upper limb amputees. Tasks such as these require accurate slip control of multiple fingertips simultaneously across different surfaces. In this paper, we explore the potential for three amputees and nine non-amputees to simultaneously control the state of sliding contact at two fingertips simultaneously by integrating two channels of variable frequency vibrotactile haptic feedback into their motor control strategies. The rendering of the man in this image was licensed and modified for public display.

There have been numerous efforts to explore noninvasive methods to increase the human-prosthesis bandwidth [8], for example, EMG pattern recognition to control a prosthetic wrist [9] while simultaneously operating a prosthetic hand. These efforts detailed multi-layer perceptron [10], linear discriminant analysis [11–13], convolutional neural networks [14], and neuromusculoskeletal models [15] to detect hand motions while wrist pronation/supination or flexion/extension motions were simultaneously performed.

There have also been prior efforts to investigate the ability for the simultaneous control of multiple grips or fingers of prosthetic hands independently via noninvasive methods [16]. One major obstacle of this goal is the substantial crosstalk that occurs between muscle recording locations on the forearm [17]. However, there has been progress to decode individual finger movements with different signal processing and machine-learning algorithms. For example, one paper has classified twelve different imagined individual finger movements from six amputees and also combined finger movements from ten limb-intact subjects; high classification accuracies for five distinct finger movements were obtained using six EMG electrode pairs [18]. For a review on EMG pattern-recognition techniques for prosthetic hand control, see [19].

Regarding the noninvasive feedback of haptic sensations, there have been myriad approaches explored in the literature, including mechanotactile [20–22], vibrotactile [20,23,24], and electrotactile feedback methods [25–27]; see [1,28,29] for reviews. Particularly relevant to this paper, vibrotactile haptic feedback has been explored due to the light weight and low power requirements of these actuators, which make them conducive to use in wearable prosthetic limbs [30]. Vibrotactile feedback can be readily integrated into artificial hand control strategies [31] and can be used to convey haptic feedback for grasped object slip sensations [28]. Furthermore, vibrotactile feedback has been shown to surpass both visual and proportional force haptic feedback in grasped object slip prevention experiments with an artificial hand [32]. The sense of object slippage is particularly important for amputees because they are often unaware of the applied grip force, leading to inadvertently dropping the grasped object [33].

While there have been numerous efforts to prevent the slip of grasped objects [34], one commonly overlooked aspect of control is that it is often desirable to permit slip to occur, such as in haptic exploration tasks [35] to manually gather information about the environment [36] with tactile sensor arrays [37], similar to how people use myriad mechanoreceptors in the human fingertips [38]. Fine details of the situation at hand can dictate whether the person would desire to prevent or permit slip [3], such as when handing an object to another person—sliding contact is likely to occur during the handoff [2].

Grasp control challenges compound when multitasking or controlling multiple functions simultaneously. Multichannel haptic feedback arrays show promise to help overcome this difficulty by conveying a broader picture of the hand to the amputee [39] from multiple fingertips simultaneously [40]. However, there is scant research investigating how well amputees can integrate myriad channels of haptic feedback into their dexterous artificial hand control strategies. The hypothesis of this paper is that amputees can integrate multiple channels of simultaneously activated haptic feedback into their concurrent control strategies for individual fingers of an artificial hand. To test this hypothesis, we developed a novel experimental paradigm where sliding contact occurred in two different directions simultaneously on two fingertips of an artificial hand, somewhat like how people slide their natural fingers in different directions simultaneously along the strings of a violin, on touch screen devices and mouse pads, or in other tasks of daily life. The sliding sensations of touch from the two robotic fingertips were encoded by the frequency of stimulation based upon the direction of slip at each fingertip and mapped to corresponding wearable vibrotactile actuators. Three amputees and nine additional subjects were fitted with an array of EMG electrodes, and muscle activation pattern recognition was implemented with an ANN to enable individual and concurrent control of two fingers of the hand. Subjects were trained to recognize the state of sliding contact at both fingertips by the context-dependent simultaneously activated haptic feedback and to decide whether to prevent or permit the slip of two different objects at the same time.

While there is extant research on EMG pattern recognition for the simultaneous multi-DOF control of artificial hands and methods for conveying multiple channels of haptic feedback to amputees, there is a dearth of research investigating amputees' capabilities for multichannel sensorimotor integration. We use the term sensorimotor integration to describe the ability of people to combine sensory input and motor output signals to internally estimate the state of the artificial hand interacting with the world [41]. The novel contribution of this paper is a demonstration of amputees' capabilities for multichannel sensorimotor integration to concurrently control the individual fingers of a dexterous artificial hand based on nuanced haptic feedback from multiple channels of simultaneously activated vibrotactile stimulators.

2. Materials and Methods

2.1. Human Subjects

Twelve human subjects participated in these experiments (six females). Three male subjects had an upper limb amputation or congenital deficiency. The first subject (S1) had

a bilateral amputation: transhumeral on the right side, transradial on the left side. He frequently uses several myoelectric and body-powered prosthetic devices with his left arm, including the Fillauer Motion Control ETD Hook with an MC wrist rotator (Fillauer, Boulder, CO, USA). The second subject (S2) has a transverse congenital limb deficiency of the left arm slightly beyond the elbow. He uses a body-powered TRS Grip Prehensor (Grip 3 BK) daily. He has used myoelectric prostheses several times in the past but has never owned one because he prefers body-powered prostheses for several reasons, including lower operational noise and cost. The third subject (S3) has a complex partial amputation of the left hand that was caused by an explosion. He does not use a prosthesis due to the difficulty of fitting a socket to his residual limb and has never used a myoelectric prosthesis. The other nine subjects (S4–S12) had no amputation or congenital limb deficiencies. All participants gave informed written consent under a protocol approved by Florida Atlantic University's IRB, which is in accordance with the declaration of Helsinki.

2.2. Robotic System Hardware

The robotic system includes an E3M Dexterous Shadow Hand (Shadow Robot Company, London, UK), fitted with BioTac SP tactile sensor arrays (SynTouch, CA, USA) on both the I and L fingertips (Figure 2A–E) [42]. The Shadow Hand has 20 tendon-driven DOFs; however, for the purpose of exploring the capacity for simultaneous slip control in this paper, only the metacarpophalangeal joints of the I and L fingers were under the control of the users, effectively limiting the DOFs to two. The BioTac SP fingertip tactile arrays are deformable fluid-filled sensors that have 24 internal electrodes with impedances that vary as external forces displace the fluid within the cavity (Figure 2A). There is also an internal piezoresistive pressure transducer (24PC15SMT, Honeywell) to measure the steady-state pressure (P_{DC}) applied to the fingertip. The transducer signal is amplified with a gain of ten and then low-pass filtered to yield a sensitivity of 21.8 mV/kPa. The dynamic pressure (P_{AC}) is gleaned from P_{DC} using a band pass filter (10 Hz to 1040 Hz) and gain of 99.1 to produce a sensitivity of 2.16 mV/kPa [37].

Two independently controlled stepper motors (Autonics A2K-M243, TEquipment, Long Branch, NJ, USA) were mounted vertically on an aluminum plate to induce slip, either up or down on the BioTacs of the I and L fingers (Figure 2B–E). The stepper motors were rigidly connected to flat rectangular surfaces that were 3D printed with PLA material using an Ultimaker S5 (Ultimaker, Zaltbommel, The Netherlands). Sliding speeds were constant at 0.5 mm/s. Each slip platform was equipped with essential components, including a stepper motor, stepper motor driver, lead screw, two linear shaft optical axes accompanied by rod rail supports, a copper nut, four bearing pillow blocks, and a flexible motor shaft coupler. The sequencing of trials was embedded into the stepper motors' codebase, dictating their movement patterns.

The two vibrotactile stimulators (PN:LS00046, OSEEP Electronics LTD) for haptic feedback from the I and L fingertips were integrated into a stretchable haptic armband made from Dragon Skin-30 (Smooth-On, Inc., Macungie, PA, USA) to deliver information to the subjects about the direction of sliding contact at the fingertips via the frequency of their actuation.

2.3. ROS Network Configuration Overview

The system was controlled through a robot operating system (ROS) network comprised of five nodes (Figure 3). The first three ROS nodes were implemented with the Teensy 3.6 (PJRC.COM, LLC, Sherwood, OR, USA). ROS node 1 was used to control the stepper motors to initiate the slip with respect to the I and L fingers. ROS node 2 was used to control the actuation frequency of the haptic feedback from the vibrotactile stimulators [43] to correspond to either slip in the up or down directions at the I and L fingertips [2]. ROS node 3 was used to sample six EMG signals from the forearms of the human subjects for efferent control of the Shadow Hand to prevent or permit slip with each finger individually or simultaneously. ROS node 4 was deployed in MATLAB/Simulink to implement ANNs

to classify the efferent EMG signals and afferent BioTac SP fingertip slip sensations. ROS node 5 controlled the Shadow Hand.

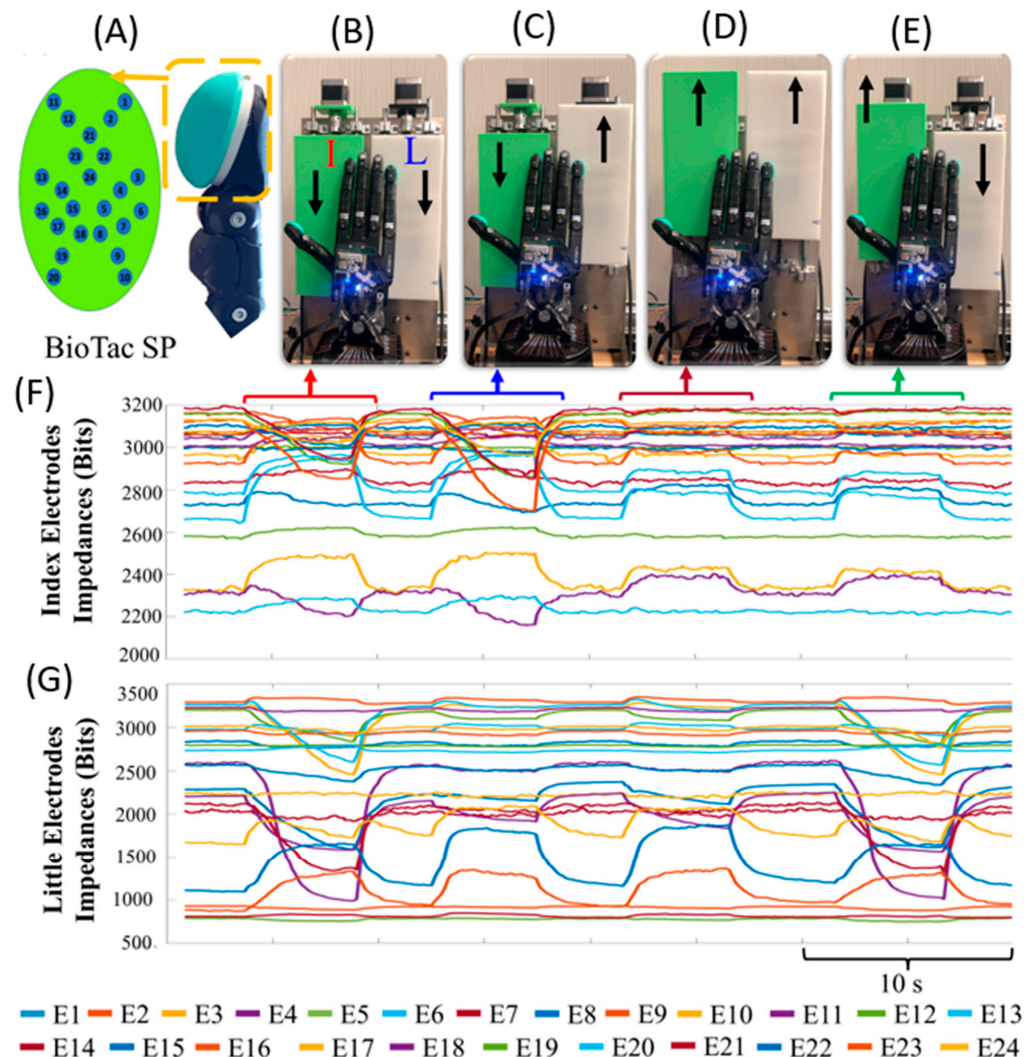


Figure 2. (A) The BioTac SP has 24 sensing electrodes. (B) Photo sequence showing the Shadow Hand in contact with the sliding surfaces. Both the sliding surfaces are slipping down. (C) The index (I) finger surface is slipping down while the little (L) finger surface is slipping up. (D) Both sliding surfaces are slipping up. (E) The I finger surface is slipping up while the L finger surface is slipping down. (F) BioTac SP electrode impedances of the I and (G) L fingers changed characteristically during the different slipping scenarios.

2.4. Classifying Context-Dependent Slip Sensations from Two Fingertips Simultaneously

BioTac sensors have been used in conjunction with ANNs to detect the incipient slip of grasped objects [44]. In this paper, we used two ANNs to classify the direction of slip on two fingertips simultaneously. To that end, data were collected from the BioTac SP sensors attached to the I and L fingers (Figure 2F,G). After establishing contact between the fingertips and the sliding surfaces, ten slip trials were induced in both the up and down directions. The two ANN classifiers for the two fingertips were designed with one input layer, one hidden layer, and one output layer. There were 24 neurons on the input layer corresponding to the 24 taxels in each BioTac SP (Figure 2A) and two neurons in the output layer for the slip-up or slip-down classes. There were 100 neurons in the hidden layer. Sigmoid and SoftMax activation functions were used for the hidden layer and the output layer, respectively. Cross-entropy and confusion matrices were used to evaluate the performance of the ANNs. The networks were trained with scaled conjugate gradient

backpropagation using the nprtool in MATLAB. To train and test the ANNs, the collected data were divided into 3 categories: training, testing, and validation. The ANNs were trained using 70% of the data and the network was adjusted based on the error generated from this dataset. Network generalization was measured using the 15% validation dataset, and the training was halted when the generalization error stopped improving. The 15% testing dataset did not affect the network error and provided a new performance measure that was independent from the training and validation performance measure. See our prior work for more details on the process to classify the direction of sliding contact with ANNs [2].

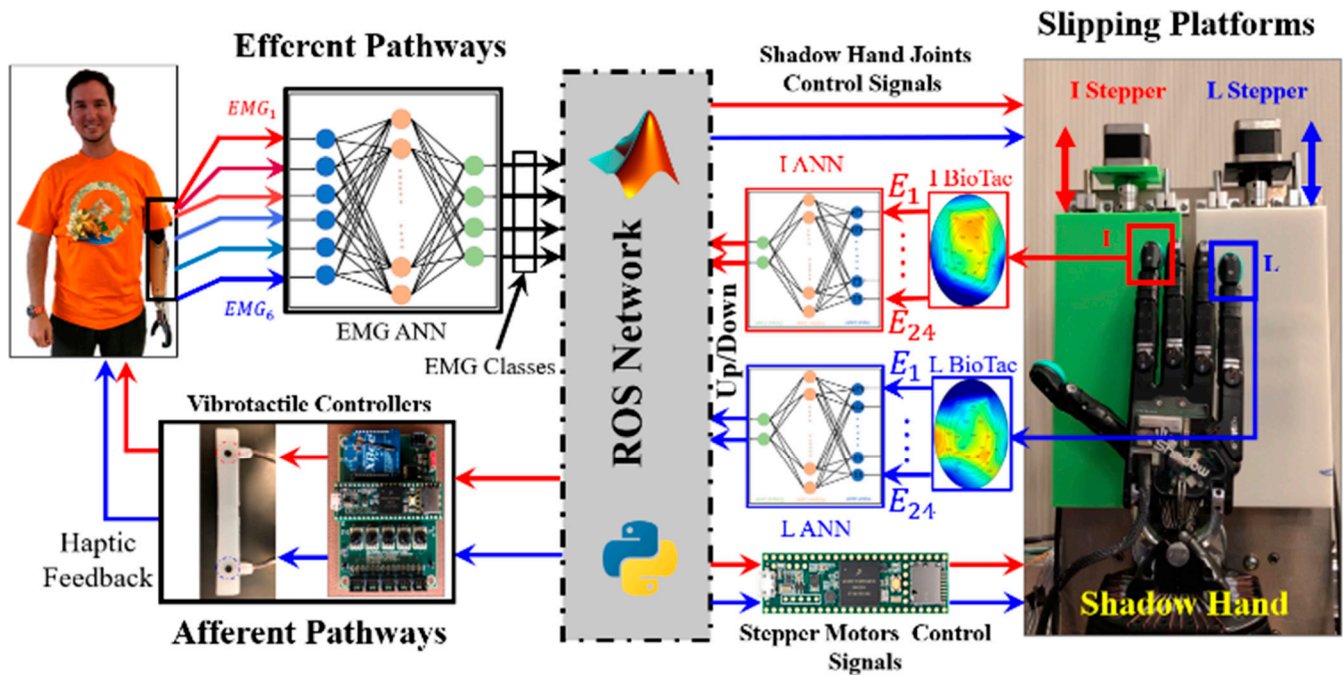


Figure 3. The robotic system configuration. All the system components are interacting with each other through ROS using Python and MATLAB/Simulink. The subject (S2) gave permission for the use of his image.

2.5. Haptic Encoding of Task-Relevant Slip Sensations from Two Fingertips Simultaneously

In the four-channel theory of touch sensation, there are four mechanoreceptors that are divided into slowly and rapidly adapting types [45]. Slowly adapting mechanoreceptors include the Merkel disc and Ruffini endings and are thought to convey myriad types of information, like static pressure and skin stretch [38]. On the other hand, the rapidly adapting Meissner and Pacinian corpuscles are more responsive to the high-frequency vibrations that can occur during sliding contact. There are some minor discrepancies in the literature regarding the frequency ranges over which these rapidly adapting mechanoreceptors are responsive; see [38,45] for more details.

To encode a directional sense of the sliding motion at the two robotic fingertips, each vibrotactile stimulator was toggled on and off in different ways to convey upward or downward slip. For upward slip, the vibrotactile actuator drive signal was a (Slow) 1 Hz square wave with a 50% duty cycle. For downward slip, the vibrotactile actuator drive signal was a (Fast) 200 Hz square wave with a 50% duty cycle. To objectively quantify the haptic feedback encoding methods from the vibrotactile stimulators, the BioTac SP sensor was utilized as a measurement tool. To that end, the vibrotactile stimulator was connected firmly to the BioTac SP sensor on the I fingertip (Figure 4A). The Slow and Fast vibrotactile activation signals for this test were created in Simulink using the ROS toolbox. The steady-state pressure (P_{DC}) and dynamic pressure signals (P_{AC}) from the BioTac were recorded for both the Slow (Figure 4B,D) and Fast (Figure 4F,H) vibration modes.

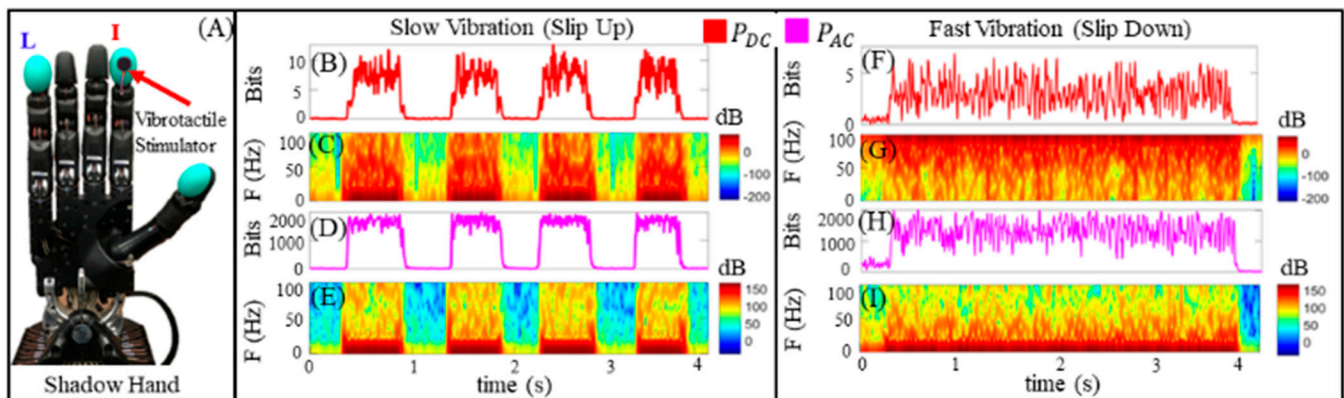


Figure 4. Characterization of the two vibration modes of the vibrotactile stimulators for haptic feedback to the human subjects from the index (I) and little (L) fingers. (A) The BioTac SP on the I finger of the Shadow Hand was used in this experiment to measure the Slow and Fast vibration modes of the vibrotactile stimulators that was conveyed to the human subjects. (B) Steady-state pressure (P_{DC}) and (C) spectrogram of the steady-state pressure (P_{DC}) measured by the BioTac corresponding to the Slow vibration mode. (D) The dynamic pressure signal (P_{AC}) and the (E) corresponding spectrogram from the Slow vibration mode. (F) Steady-state pressure (P_{DC}) and (G) spectrogram corresponding to the Fast vibration mode. (H) The dynamic pressure signal (P_{AC}) and (I) the corresponding spectrogram from the Fast vibration mode.

The time–frequency spectrogram representation for the data was calculated using a 512-point FFT with 0.08 s frame length and a Hanning window with 90% overlap. The time–frequency power distribution data show the frequency components of P_{DC} and P_{AC} for the Slow (slip up; Figure 4C,E) and Fast (slip down; Figure 4G,I) vibrotactile actuation modes. Note that the powers of these signals are broadly distributed through 100 Hz, which falls well within published accounts of human perceptual ranges [38,45,46]. These produced very different activation signatures, which enabled people to clearly distinguish between the different sensations corresponding to upward and downward sliding contact, which will be described more in Section 2.6.3.

2.6. Overview of Situationally Aware Multichannel Sensorimotor Integration Experiments for Simultaneous Slip Control

Subjects were trained over the course of approximately two hours to integrate two channels of vibrotactile haptic feedback into their simultaneous control strategies for the I and L fingers. When an object slides along a fingertip, this can be desirable or undesirable depending upon the context. For example, an object sliding upward could be caused when handing an item to another person whereas an object sliding downward could be due to inadvertently dropping an object onto the floor. In the former case, permitting slip would be desirable to hand an object to the other person. In the latter situation, it would be desirable to prevent slip by increasing the grip force. We simulated these scenarios and encoded the vibrotactile actuation frequency from the I and L fingertips to be either Slow (Figure 4B–E) or Fast (Figure 4F–I) to correspond to the slip up or slip down cases, respectively. In the slip up case, subjects were trained to permit slip while in the slip down situation subjects were trained to increase the grip force of the corresponding finger. This necessitated training the subjects to simultaneously interpret the two channels of context-dependent haptic feedback to make the corresponding control actions with both fingers concurrently. To achieve this feat of multichannel sensorimotor integration, an ANN for efferent control was developed for EMG pattern recognition with each subject. Next, subjects were trained to interpret the haptic feedback sensations from each fingertip, first individually, and then simultaneously. Finally, the multichannel sensorimotor integration experiments with the entire robotic system were performed.

2.6.1. Training for Simultaneous EMG Slip Control

Six EMG signals were recorded from the forearms of each human subject (four electrodes are 13E200 AC, Otto Bock, and two electrodes are from Myolab II (Motion Control, Inc., Salt Lake City, UT, USA)). These electrodes had internal electronics to amplify, filter, and rectify the raw EMG. The six electrodes were arranged circumferentially around the forearm roughly 7 cm below the elbow, with an approximately equal distance between each electrode (Figure 5C). The EMG recording sites for subject S3 were underneath the purple armband shown in Figure 5C. The locations of EMG recording sites for subject S1 were underneath the black armband on his residual limb, shown in Figure 6. Care was taken to place three EMG electrodes atop muscles in the anterior compartment and three electrodes over muscles in the posterior compartment of the forearm to target both the extensor and flexor muscles of the little and index fingers. The subjects were asked to flex muscles in their forearms to ensure that all signals responded well and to fine-tune electrode locations and gains. At this stage, we also verified that EMG signal amplitudes responded differently to the real and imagined I/L finger movements of the non-amputee and amputee subjects, respectively.

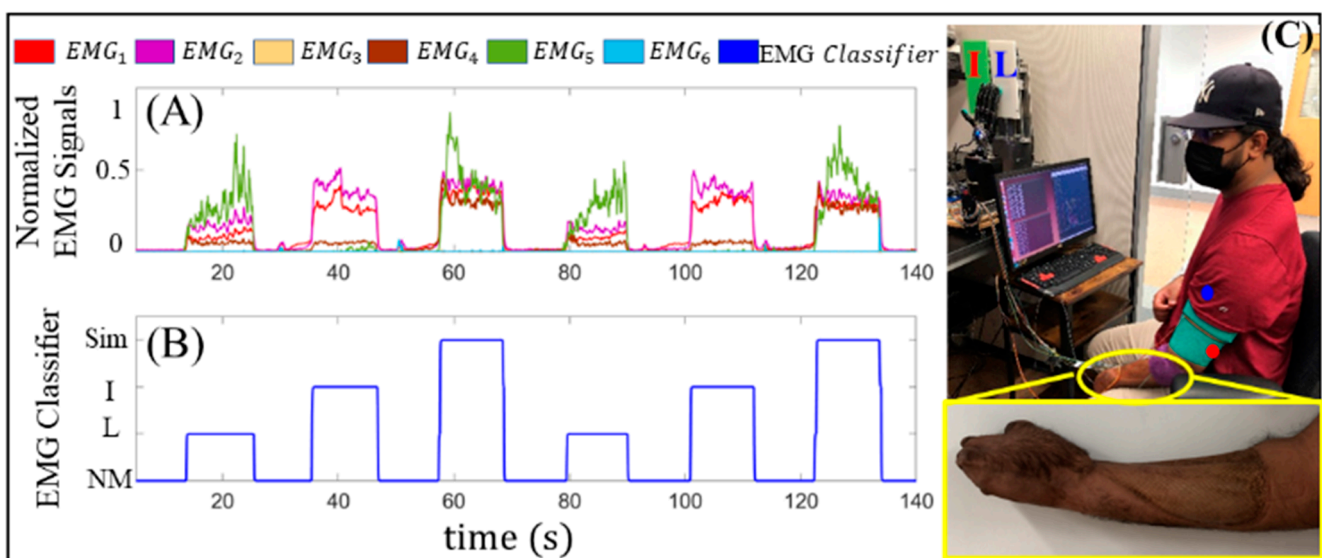


Figure 5. Training subjects for efferent control. (A) The amplified, filtered, and rectified EMG signals from six electrodes were normalized. (B) ANN classifier outputs for the Sim, I, L, and NM classes corresponding to the six EMG signals. (C) Subject S3 performing the EMG classifier training. The red and blue circles indicate where the vibrotactile stimulators for the index (I) and little (L) fingers were respectively placed for subject S3. The subject (S3) gave permission for the use of his image.

Next, ANN classifiers were trained for each subject, with six EMG inputs and four output classes. The outputs from the ANN classifier were No Motion (NM), Index (I) finger flex, Little (L) finger flex, and Simultaneous (Sim) finger flexion of both the index and little fingers (Figure 5A,B). For each class, 10 trials were collected in which the human subjects were asked to follow a 0.1 Hz square wave with 50% duty cycle generated in Simulink that was displayed on the monitor in front of them (Figure 5C). The amplified, filtered, and rectified EMG time domain data were used to train the subject-specific ANN classifiers for EMG pattern recognition. EMG data were separated into four different matrices corresponding to each class and were labeled to train the ANN classifier offline using the same methods previously described for the tactile slip sensation classification problem described in Section 2.4; however, in this case, there were six neurons on the input layer corresponding to the six EMG signals and four neurons in the output layer for the four classes. After the ANN was trained for each subject, the high functionality of the

classifier was quickly verified in real time in Simulink by asking every subject to produce each EMG class several times before the robotic experiments took place (Figure 5C).

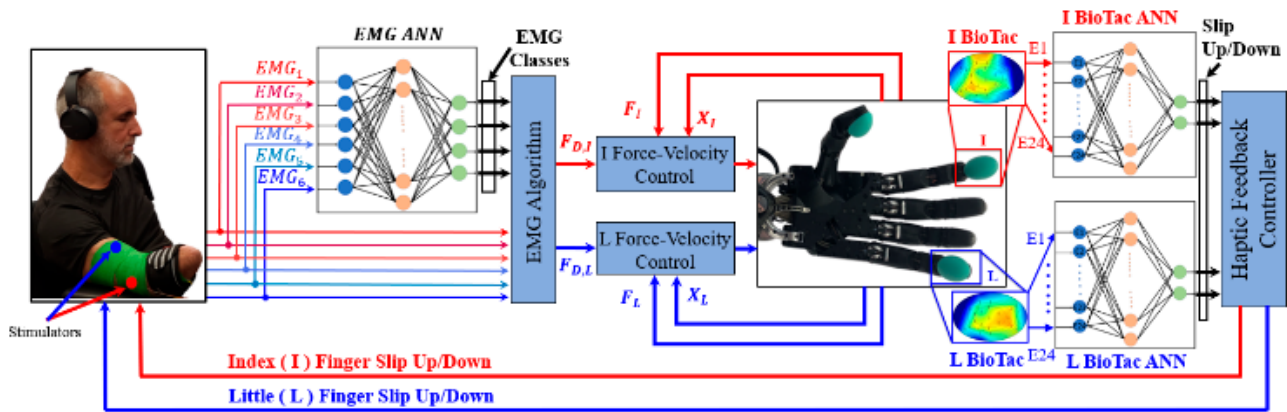


Figure 6. Control system for multichannel sensorimotor integration. Six EMG signals were classified by subject-specific ANNs to specify which finger(s) the subjects wanted to control. The EMG signals were also used to specify the desired forces for the index (I) and little (L) fingers that were realized by hybrid force–velocity controllers. ANNs were used with the BioTac SPs on the I and L fingers to classify the 24 taxels at each fingertip into sensations of sliding contact, either up or down. These sensations of touch from each fingertip were encoded via the frequency of vibration and fed back to the subjects with the haptic armband. The red and blue circles indicate where the vibrotactile stimulators for the index (I) and little (L) fingers were respectively placed for subject S1. EMG electrodes were located under the black armband. The subject (S1) gave permission for the use of his image.

2.6.2. EMG Control Algorithms for Simultaneous Slip Prevention

EMG signal processing to control slip simultaneously or individually with two fingers independently or concurrently was accomplished first by normalizing the EMG signals from each electrode. Next, the desired force ($F_{D,\varnothing}$) for the index (I) or little (L) finger ($\varnothing \in I, L$) was specified as:

$$F_{D,\varnothing} = \beta_{\varnothing} \sigma_{\varnothing} E_{\varnothing}. \tag{1}$$

β_{\varnothing} was the desired force gain for finger \varnothing . The σ_{\varnothing} term was specified by a look-up table that was based on the EMG class (Table 1) to determine which finger(s) the subject desired to control. E_{\varnothing} was the mean of the normalized voltages from the six EMG electrodes.

Table 1. Correlation between EMG class from the efferent ANN and the desired force ($F_{D,\varnothing}$) for each finger $\varnothing \in I, L$.

EMG Class	Index Finger (σ_I)	Little Finger (σ_L)
NM	0	0
Sim	1	1
L	0	1
I	1	0

The two desired forces ($F_{D,\varnothing}$) were inputs to two hybrid force–velocity controllers [47] that were implemented in MATLAB/Simulink to control the I and L fingers (Figure 6). The two different controllers for each finger had an outer force feedback loop and an inner velocity feedback control loop. The two hybrid force–velocity controllers for the I and L fingers were designed as described in our prior work [40]. Summarizing, the outer force feedback loop for each fingertip used the corresponding BioTac P_{DC} value to control the applied fingertip force and the measured joint angles (X_{\varnothing}) to control the velocity.

2.6.3. Learning Context-Dependent Multi-Digit Haptic Feedback

Training the subjects to interpret the context-dependent haptic feedback from the vibrotactile stimulators was the next step. For the congenitally limb-absent subject S2 and the nine non-amputee subjects S4–S12, the vibrotactile stimulators were placed on the upper arm over the biceps and triceps for haptic feedback corresponding to the I and L fingers, respectively. However, the amputee subjects S1 and S3 had poor sensitivity in several locations on their upper arms due to scar tissue and requested different haptic feedback locations. After a brief searching process, suitable haptic feedback sites were identified nearer the deltoid and elbow.

The haptic feedback training process started by demonstrating the Slow and Fast vibrotactile stimulator activation modes through Simulink in real time. These two frequencies of activation produced different vibratory sensations (Figure 4). For example, the amplitude of the steady-state pressure (P_{DC}) at the Fast frequency (Figure 4F) was approximately half that of the Slow activation frequency (Figure 4B). The power spectral distribution of each vibration mode was quite different for both P_{DC} (Figure 4C,G) and P_{AC} (Figure 4E,I), which also helped produce distinguishable haptic signatures for each vibration mode.

Next, the subjects were told the correlation between the Fast/Slow vibration modes and the direction of slip at the fingertips. Specifically, the Slow vibration mode indicated upward slip, while the Fast vibration mode indicated downward slip. After describing this mapping to the human subjects, their haptic perception was systematically tested. A pseudo-random sequence of 25 trials was generated using the MATLAB randperm command to test their ability to simultaneously detect the directions of slip from both vibrotactile stimulators at the same time. There were five repetitions of each of the five possible combinations of simultaneous vibration activation modes (Table 2). All subjects were able to correctly interpret the simultaneous vibrotactile activation modes with 100% accuracy due to the significantly different sensations produced by the Slow and Fast frequencies of actuation (Figure 4).

Table 2. Sensation and action scenarios during the simultaneous slip experiments that required multichannel sensorimotor integration with the index (I) and little (L) fingers.

Haptic Feedback		Slip Sensation		Actions		Correct EMG Class
I	L	I	L	I	L	
Slow	Slow	↑	↑	x	x	NM
Fast	Fast	↓	↓	✓	✓	Sim
Slow	Fast	↑	↓	x	✓	L
Fast	Slow	↓	↑	✓	x	I
Off	Off	None	None	x	x	NM

2.6.4. Multichannel Sensorimotor Integration

Next, the four different combinations of simultaneous slip up/down with the I/L fingers were demonstrated several times for the subjects with the robotic system that was under EMG control. Subjects were allowed approximately five minutes to gain familiarity with multichannel sensorimotor integration using the robotic system to learn how the EMG control signals would stop slip of the two objects individually or simultaneously when desired. After this initial training phase, an opaque blockade was placed between the Shadow Hand and the subjects to prevent them from seeing the robotic system, forcing them to rely purely on haptic feedback. The human subjects were also asked to wear noise-cancelling headphones (Figure 6).

During the experiments, the different combinations of simultaneous slip modes were tested with a pseudo-random sequence of 50 trials (10 repetitions for each of the five options listed in Table 2, including the option where haptic feedback was disabled). All the human subjects went through the same pseudo-random sequence that was generated with the

MATLAB randperm command. The subjects controlled the pace of the experiments by pressing the Enter key on the keyboard in front of them to initiate each trial. Every trial was designed to be 15 s long, during which subjects were asked to perceive the nuanced multichannel haptic feedback and appropriately respond to the sensations with the correct EMG control classes. They were trained to permit upward slip at the finger(s) where they perceived upward slip and conversely to prevent slip at the finger(s) where they sensed downward slip (Table 2). Subjects progressed through these 50 trials in approximately 45–60 min, with short rest breaks whenever requested.

The metric to quantify how successful the subjects were with this feat of multichannel sensorimotor integration was calculated as the percentage of time that the subjects maintained the correct EMG class during each 15 s trial after they responded to the simultaneous slip haptic feedback stimuli. The 15 s time window allowed sufficient time for each subject to perceive and respond to the haptic sensations and provided an appropriate challenge for subjects to maintain the correct class. Additionally, the response time (RT) was computed for each subject and class as the amount of time each person required to interpret the haptic feedback and respond, in other words, the time difference between the onset of haptic feedback and activation of an EMG class (Figure 7H,J). The human reaction time to haptic stimuli has often been used as a metric of the cognitive load to operate a prosthetic hand [48,49].

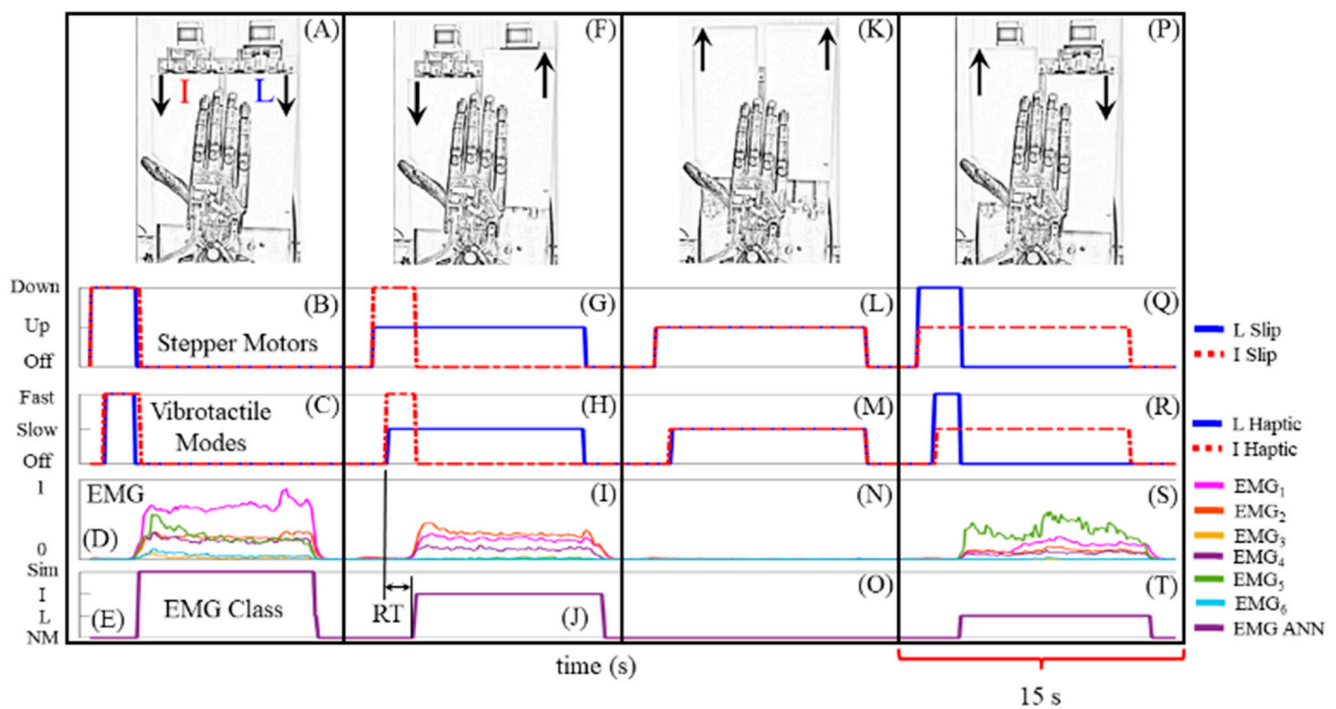


Figure 7. Sample data illustrating robotic system operation for the four cases of simultaneous slip at the index (I) and little (L) fingers. Simultaneous haptic feedback had two different vibration frequencies depending upon the direction of sliding contact. Upward slip was encoded with Slow vibration, while the downward slip produced Fast vibration. Subjects were trained to permit upward slip but prevent downward slip using their six EMG signals to produce four different classes (Sim, I, L, NM) with the efferent ANN. (A) Simultaneous downward slip at each fingertip was created by (B) both stepper motors driving downward slip. (C) This caused both vibrotactile actuators to be activated in the Fast mode. (D) The subject perceived the simultaneously activated channels of haptic feedback and increased his EMG signals (E) to produce the Sim class with the efferent ANN. (F,G) Slip down at the I finger with slip up at the L finger caused the (H) vibrotactile stimulators to be actuated with the Fast and Slow modes, respectively. (I) The subject responded to this multichannel

haptic feedback to increase his EMG signals and (J) produced the I class. (K,L) Simultaneous upward slip at each fingertip (M) caused both vibrotactile stimulators to be actuated with the Slow mode. (N) The subject did not increase his EMG signals since he desired slip to occur at both fingertips in this case (O), producing the NM class. (P,Q) Slip up at the I finger but slip down at the L finger (R) produced the Slow and Fast vibrational frequencies for the I and L haptic feedback, respectively. (S) The subject responded to this haptic feedback by increasing his EMG signals (T) to produce the L class. The response time (RT) is calculated as the time difference between the onset of haptic feedback and when the subject produced an EMG class (H,J).

For both dependent variables (multichannel sensorimotor integration success rate, RT), two-factor ANOVA was performed in MATLAB with human subject and EMG class as the two independent variables. Interaction between the human subjects and EMG class was also tested for statistically significant impact upon the multichannel sensorimotor integration success rate and RT. An unbalanced ANOVA was also performed to determine if there was a statistically significant difference between amputee and non-amputee subjects for both dependent variables.

3. Results

Sample data show the four possible cases of simultaneous slip at the I and L fingers (Figure 7). When both stepper motors drove the slip platforms downward (Figure 7A,B), the afferent ANNs correctly classified the sensations and the vibrotactile actuators corresponding to the I and L fingers were both activated in the Fast frequency (Figure 7C). This prompted the subject to increase his EMG signals (Figure 7D) to produce the Sim class (Figure 7E) using the efferent ANN, which caused both the slip (Figure 7B) and haptic feedback to cease (Figure 7C). When the sliding contact at the I finger was downward while slip at the L finger was concurrently upward (Figure 7F,G), the vibrotactile actuator corresponding to the I finger was actuated in the Fast mode while the corresponding haptic feedback from the L finger was actuated simultaneously in the Slow mode (Figure 7H). This caused the subject to increase his EMG signals (Figure 7I) to produce the I class using the EMG ANN (Figure 7J), which halted slip at the I finger (Figure 7G) and the corresponding haptic feedback from the I finger; the haptic feedback from the L finger remained on in the Slow mode since the user desired to permit slip at the L finger only (Figure 7H). When slip at both fingertips was upward (Figure 7K,L), both vibrotactile stimulators were actuated in the Slow mode (Figure 7M) and the subject chose to take no action (Figure 7N), which produced the NM class (Figure 7O) to permit slip at both fingers in this situation (Figure 7K,L). When slip at the I finger was upward, while slip at the L finger was simultaneously downward (Figure 7P,Q), the afferent ANNs classified this correctly and triggered the corresponding vibrotactile stimulators to be actuated in the Slow and Fast modes to supply haptic feedback from the I and L fingers, respectively (Figure 7R). This prompted the subject to increase his EMG signals (Figure 7S) to produce the L class (Figure 7T), which halted slip at the L finger only (Figure 7Q,R).

3.1. Multichannel Sensorimotor Integration Success Rate

All participants achieved high success rates of multichannel sensorimotor integration, with an overall mean of $94.49\% \pm 8.79\%$ (Figure 8). The subject with the highest success rate was S2, with an average of $98.18\% \pm 3.14\%$, while the subject with the lowest success rate was S1, with a mean of $89.27\% \pm 15.96\%$. Averaged across all 12 subjects, the highest success rate within an EMG class was the NM class with 100% mean, while the success rates for the I, L, and Sim classes were $94.93\% \pm 11.95\%$, $91.72\% \pm 13.26\%$, and $91.30\% \pm 9.94\%$, respectively (Table S1).

The ANOVA showed that there was no significant difference between the subjects' success rates or the different classes ($p > 0.05$). However, the interaction between subjects and classes was significant ($p < 0.05$). An example of this interaction can be seen with subject S8, who had a lower success rate with the Sim class, while subject S10 had lower success rate with the L class.

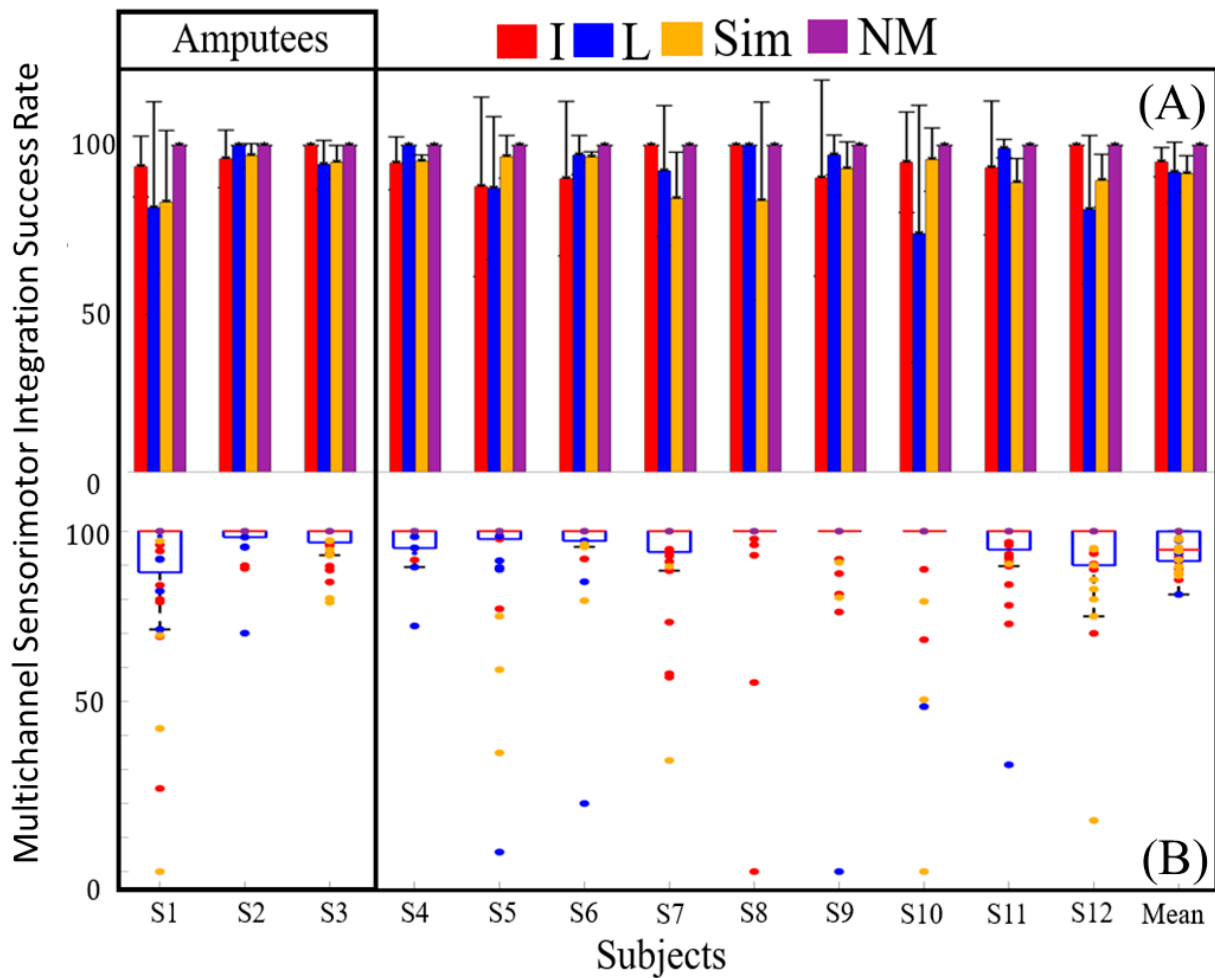


Figure 8. (A) Multichannel sensorimotor integration success rates for all subjects with each class demonstrated high proficiency for sensorimotor integration. (B) Box plots showing multichannel sensorimotor integration success rates for each trial with all the subjects.

The mean multichannel sensorimotor integration success rate for amputees was $94.90\% \pm 7.43\%$, while the average for the non-amputees was $94.36\% \pm 9.24\%$. The unbalanced ANOVA showed that the amputees’ average success rate was not significantly different from the non-amputees ($p > 0.05$).

3.2. Response Time to Multichannel Haptic Feedback

The mean RT of the three amputees was $3.46 \text{ s} \pm 0.82 \text{ s}$, while the mean RT for non-amputee subjects was $2.42 \text{ s} \pm 0.63 \text{ s}$ (Figure 9). The average RT across all 12 subjects was $2.68 \text{ s} \pm 0.68 \text{ s}$. Subject S4 had the fastest mean RT of $1.50 \text{ s} \pm 0.45 \text{ s}$, while subject S1 had the slowest RT of $3.83 \text{ s} \pm 1.13 \text{ s}$. The three amputee subjects (S1–S3) had the three slowest average RTs within the cohort (Table S2).

The ANOVA on the RT across all subjects showed a statistically significant difference ($p < 0.01$). The RT for each class was also statistically significant ($p < 0.01$). However, the interaction between the subject’s performance and the classes was not statistically significant ($p > 0.05$). The unbalanced ANOVA showed that the amputee RT was significantly different than the non-amputee RT ($p < 0.01$).

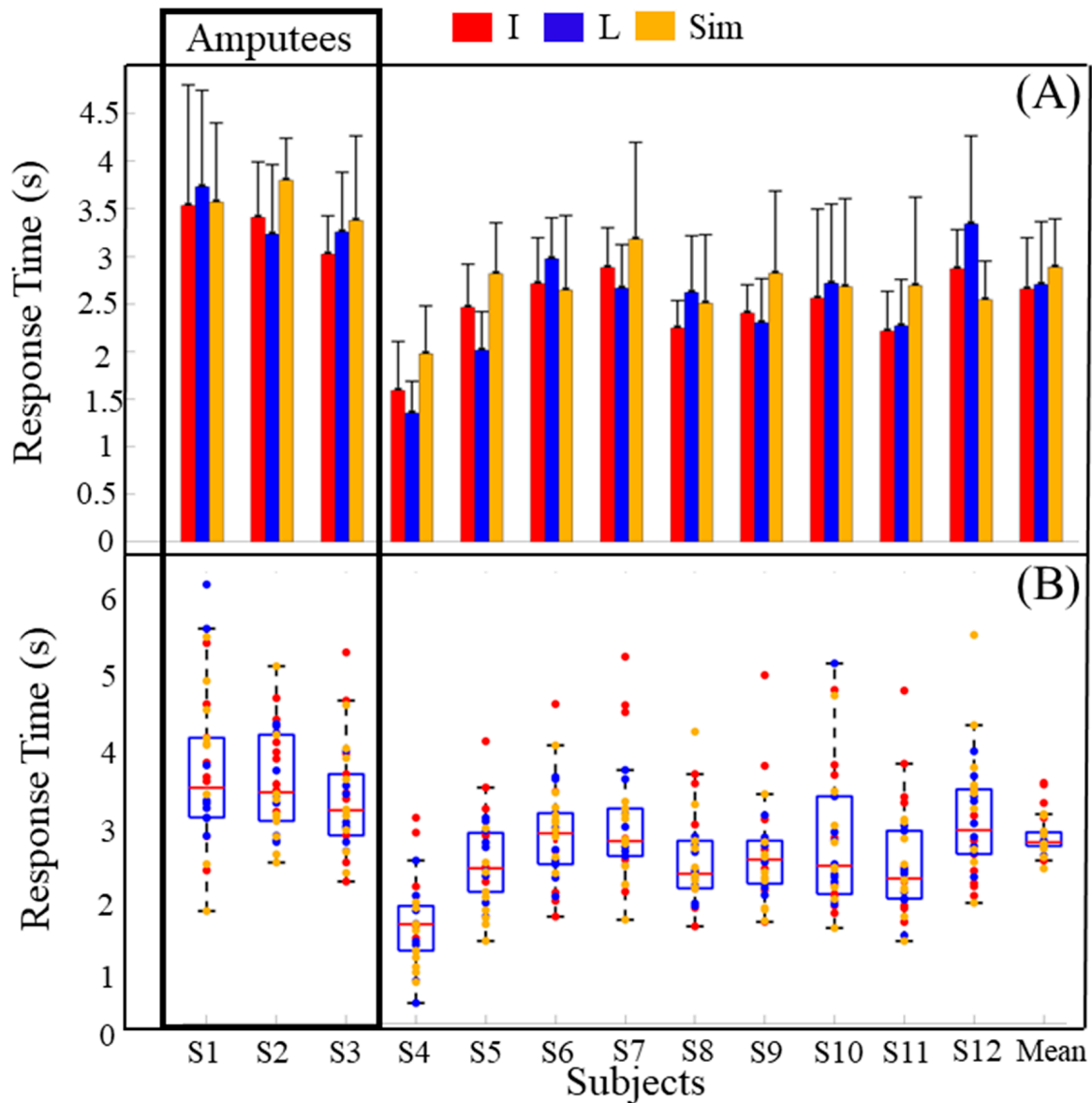


Figure 9. (A) Each subject’s response time for the I, L, and Sim classes. (B) Box plots for every subject’s response times with each class. The amputees had a significantly longer time to respond to the haptic stimuli than the non-amputees.

4. Discussion

EMG pattern recognition research for amputees’ control signals has led to several commercially available products from Otto Bock [50] and Coapt [51] for the control of multiple DOFs of a prosthetic arm. However, haptic feedback for amputees in clinical practice is largely unrealized, with few exceptions, for example, the Psyonic Ability hand [52] and the Vincent evolution hand [53], which both offer some rudimentary capacity for vibrotactile sensations. The explanation for this dearth of sensation is multifaceted [1], but since several prosthetic hands already have vibrotactile feedback capabilities, the technical barriers to clinically implement the haptic feedback system described in this paper largely stem from the lack of appropriate sensors on prosthetic fingertips. Unfortunately, most prosthetic hands still do not have tactile sensors [54,55]. At present, there are no practical commercial tactile sensors available for prosthetic hands that can detect sophisticated sensations like the direction of sliding contact. Another consideration to implement multichannel haptic feedback is that prosthetists would need to work with their patients to identify appropriate feedback locations and be equipped with the tools for customizing prosthetic sockets to

accommodate individualized haptic feedback arrays. Nevertheless, enhancement of artificial hand sensation and haptic feedback will be impactful to improve prosthetic arm embodiment [56] and reduce the prevalence of artificial limb rejection [57], which remains high because of poor dexterity and lack of sensory feedback, among other reasons [58].

Dexterous prosthetic hands of the future will also require more sensory feedback to improve their functionality, but this must be balanced against excessively increasing their cognitive operational burden. The amount of time people require to respond to haptic stimuli has been used as a metric indicative of the cognitive load to operate a prosthetic hand [48,49]. Haptic feedback from a single channel can help reduce the cognitive load to perform a single task. For example, it has been shown that amplitude modulation from a single vibrotactile stimulator can help reduce reaction time and cognitive load compared to spatially encoding the feedback via multiple stimulators [59]. However, the cognitive load will increase when scaling up the number of feedback channels [29]. In our paper, we used two channels of haptic feedback that were simultaneously activated with frequencies dependent upon the direction of sliding contact. The ANOVA showed a statistically significant impact of the simultaneous vibration mode upon the RT ($p < 0.05$; Figure 9). In particular, the Sim class had the slowest RT averaged across all subjects, and this is the situation where both vibrotactile stimulators were activated with the same Fast frequency. The other situations requiring an action from the subjects (I, L classes in Figure 9) had both the Slow and Fast frequencies of vibration simultaneously from the two stimulators, and so could have been easier for most subjects to discern more rapidly. In those situations, one stimulator was activated during downward slip (Figure 4F,H), while the other was toggled on and off every 500 ms to indicate upward slip (Figure 4B,D). Subjects S6 and S12 were the only two people who had the fastest mean RTs with the Sim class; the other ten subjects responded more quickly on average in situations where the frequencies of vibration from the two stimulators were different (I,L classes).

Shah et al. described a relevant finding in their study involving people's capacity for discriminating between simultaneously and sequentially activated vibrotactile stimulators [60]. Specifically, their subjects were on average less sensitive to differences in stimulation frequency between the two actuators when they were simultaneously driven in comparison to when they were sequentially activated with a 750 ms interstimulus interval. One possible explanation for the similar results in [60] and our data could be caused by dual task interference described by the so-called psychological refractory period [61], which is a slowing that occurs when people try to do two tasks simultaneously [62]. The human capacity for attention is a limited resource—when attention is distributed across multiple stimuli simultaneously, the capability for perception of each individual stimulus is diminished [62]. In our paper, the I and L classes each involved both the Fast and Slow patterns of vibrotactile stimulation (the Slow pattern was toggled on and off as shown in Figure 4B–E). During the time intervals in which the Slow stimulator was off, the subjects would have potentially been able to fully allocate their attention to the other active vibrotactile actuator, decide about its actuation mode, and then refocus their attention back to the opposite vibrotactile actuator when it was subsequently reactivated. In contrast, the SIM mode had both actuators constantly vibrating at the same Fast frequency, potentially leading to a central bottleneck of information processing [61] that could have slowed most subjects' responses relative to the other asymmetric classes (I, L). Another perceptual model on this topic compared information processing within the central nervous system to a queuing network system wherein information pertaining to each individual stimulus must pass serially through the 'server'. In this model, one of the simultaneously activated stimuli would be stored temporarily, while each stimulus is transmitted individually, increasing the RT during the queue time. In contrast, sequentially activated stimuli can be transmitted with less delay so long as a minimum interstimulus threshold of time is not exceeded [63]. The RT in this scenario is inversely related to the time difference between the initiation of the two stimuli, which is referred to as stimulus onset asynchrony—in general, the shorter the stimulus onset asynchrony, the longer the RT will be to the second stimulus. However,

understanding the cognitive processes involved in multitasking experiments remains an active area of research [64]. In the future, a detailed study systematically investigating the RT to multiple channels of haptic feedback relative to the stimulus onset asynchrony would be helpful considering the important ramifications this could have upon dexterous artificial hand control. Furthermore, there are numerous other factors that significantly affect the RT to vibrotactile feedback, including the size and type of actuator that is used, the locations where they are placed, vibration frequency and amplitude [65], the cognitive load during use, and the age of the subject [66]. Other factors that could impact the RT to haptic feedback include the modality of haptic feedback [20,67], whether to encode tactile events spatially or temporally [59], and the number of independent haptic feedback channels [29].

Additionally, it would be valuable to consider experiments in unstructured situations where slip could occur in any direction and to evaluate how haptic feedback would impact subjects' performances when they are able to see the hand. It is likely that visual feedback would have improved the RT of the subjects in this study; however, our focus in this paper was to discover if subjects could interpret two channels of simultaneously activated haptic feedback while concurrently controlling two fingers in the absence of visual feedback. This commonly occurs at night, when performing complex tasks like sports, playing musical instruments, or during bimanual tasks in which both hands cannot be simultaneously monitored visually.

On the efferent side, EMG pattern-recognition approaches can reduce the cognitive load required to operate myoelectric hands [68], but there are some differing reports regarding the utility of this approach for amputees relative to non-amputees. For example, a comparison between two amputees and 12 non-amputees showed that amputees had a lower success rate and required more time to complete a pick and place task with different objects using a regularized discriminant analysis grip classification algorithm and a hybrid EMG-inertial measurement unit sensor suite [69]. In contrast, another study used a KNN algorithm for EMG pattern recognition in which no statistically significant difference was found between non-amputees and amputees for the time needed to select a desired motion of myoelectric prostheses [70]. The data in our paper support the idea that amputees may have a higher cognitive load required in sensorimotor integration tasks involving the pattern recognition of multiple channels of efferent and afferent information relative to non-amputees. This is suggested by the fact that the three amputees in our study had a significantly slower RT to perform the multitasking experiments in comparison to the nine non-amputees (Figure 9; $p < 0.01$); the amputees' EMG classification accuracies were not significantly different from the non-amputees (Figure 8; $p > 0.05$). However, additional experiments should be carried out with a larger sample size to explore the impact of congenital or traumatic hand amputation upon the cognitive load required to operate dexterous prostheses.

A traumatic upper limb amputation drives a large-scale cortical reorganization, extending well beyond the sensorimotor cortex [71], which could have affected the RT of the amputee subjects S1 and S3, who both suffered amputations as adults. One confounding factor is the possibility that the different vibrotactile feedback sites requested by subjects S1 and S3 could have affected their RTs. This is because people have demonstrated different levels of sensitivity to vibrotactile feedback applied to different locations of the arm, likely due to variable distribution of Pacinian corpuscles [38] in different dermatomes of the arm [60]. However, subject S2, who has a congenital limb deficiency, also had a significantly slower RT, and he used the same vibrotactile feedback locations as the non-amputee subjects S4–S12. During development, children with congenital limb deficiencies are deprived of afferent peripheral sensations that would normally shape the function of the assumed hand territory of the brain. Instead, compensatory movements involving the feet, lips, and forearm may provide afferent inputs to this region of the brain during maturation [72]. It therefore stands to reason that providing haptic feedback to children who are born without a hand could be beneficial to their future potential as adults.

5. Conclusions

We have developed a novel artificial hand control system demonstrating that amputees can interpret multiple channels of context-dependent haptic feedback from two different vibrotactile stimulators simultaneously to concurrently control individual fingers of a dexterous artificial hand (Figure 8). We explored the potential of three amputees and nine non-amputees to perform this complex feat of multichannel sensorimotor integration in the context of deciding whether to permit or prevent sliding contact at two fingertips of an artificial hand simultaneously. This kind of situational awareness underpins the refined manual dexterity inherently required to perform sophisticated tasks such as playing sports or a musical instrument, like a violin (Figure 1). Our results showed that the subjects were able to correctly interpret the vibrotactile feedback from both haptic feedback channels simultaneously to concurrently control two fingers of the artificial hand with a $94.49\% \pm 8.79\%$ success rate averaged across all 12 subjects. There was no statistically significant difference in the multichannel sensorimotor integration success rates between the amputees and non-amputees; however, the amputees did require significantly more time to respond to the haptic stimuli in comparison to the non-amputees. This suggests that the amputees might have experienced a higher cognitive load to perform the same sensorimotor integration task that required interpretation of two channels of haptic feedback simultaneously. These results provide a small step towards the grand challenge of enabling amputees to dexterously control prosthetic hands.

Supplementary Materials: The following supporting materials can be downloaded at: <https://www.mdpi.com/article/10.3390/robotics13070097/s1>, Figure S1: Experimental Workflow; Table S1: Multichannel Sensorimotor Integration Success Rate Percentage; Table S2: Response Time.

Author Contributions: Conceptualization, M.A.A. and E.D.E.; methodology, M.A.A. and E.D.E.; software, M.A.A. and E.D.E.; validation, M.A.A. and E.D.E.; formal analysis, M.A.A. and E.D.E.; investigation, M.A.A. and E.D.E.; resources, M.A.A. and E.D.E.; data curation, M.A.A. and E.D.E.; writing—original draft preparation, M.A.A. and E.D.E.; writing—review and editing, M.A.A. and E.D.E.; visualization, M.A.A. and E.D.E.; supervision, E.D.E.; project administration, E.D.E.; funding acquisition, E.D.E. All authors have read and agreed to the published version of the manuscript.

Funding: The research reported in this study was supported by the National Institute of Biomedical Imaging and Bioengineering of the National Institutes of Health under Award Number R01EB025819. This research was also supported by the National Institute of Aging under 3R01EB025819-04S1, National Science Foundation awards #2205205 and #1950400, and pilot grants from Florida Atlantic University's College of Engineering and Computer Science, the Stiles–Nicholson Brain Institute, the Center for Smart Health, and I-SENSE. The content is solely the responsibility of the authors and does not necessarily represent the official views of the National Institutes of Health or the National Science Foundation.

Data Availability Statement: The raw data supporting the conclusions of this article will be made available by the authors on request.

Conflicts of Interest: The authors declare no conflicts of interest.

References

1. Sensinger, J.W.; Dosen, S. A review of sensory feedback in upper-limb prostheses from the perspective of human motor control. *Front. Neurosci.* **2020**, *14*, 345. [[CrossRef](#)] [[PubMed](#)]
2. Abd, M.A.; Gonzalez, I.J.; Colestock, T.C.; Kent, B.A.; Engeberg, E.D. Direction of slip detection for adaptive grasp force control with a dexterous robotic hand. In Proceedings of the 2018 IEEE/ASME International Conference on Advanced Intelligent Mechatronics (AIM), Auckland, New Zealand, 9–12 July 2018; IEEE: Piscataway, NJ, USA, 2018; pp. 21–27.
3. Zangrandi, A.; D'Alonzo, M.; Cipriani, C.; Di Pino, G. Neurophysiology of slip sensation and grip reaction: Insights for hand prosthesis control of slippage. *J. Neurophysiol.* **2021**, *126*, 477–492. [[CrossRef](#)] [[PubMed](#)]
4. Johansson, R.S.; Birznieks, I. First spikes in ensembles of human tactile afferents code complex spatial fingertip events. *Nat. Neurosci.* **2004**, *7*, 170–177. [[CrossRef](#)] [[PubMed](#)]
5. Johansson, R.S.; Flanagan, J.R. Coding and use of tactile signals from the fingertips in object manipulation tasks. *Nat. Rev. Neurosci.* **2009**, *10*, 345–359. [[CrossRef](#)] [[PubMed](#)]

6. Häger-Ross, C.; Cole, K.J.; Johansson, R.S. Grip-force responses to unanticipated object loading: Load direction reveals body-and gravity-referenced intrinsic task variables. *Exp. Brain Res.* **1996**, *110*, 142–150. [[CrossRef](#)]
7. Kumar, D.K.; Jelfs, B.; Sui, X.; Arjunan, S.P. Prosthetic hand control: A multidisciplinary review to identify strengths, shortcomings, and the future. *Biomed. Signal Process. Control* **2019**, *53*, 101588. [[CrossRef](#)]
8. Wurth, S.M.; Hargrove, L.J. A real-time comparison between direct control, sequential pattern recognition control and simultaneous pattern recognition control using a Fitts' law style assessment procedure. *J. Neuroeng. Rehabil.* **2014**, *11*, 91. [[CrossRef](#)] [[PubMed](#)]
9. Bajaj, N.M.; Spiers, A.J.; Dollar, A.M. State of the Art in Artificial Wrists: A Review of Prosthetic and Robotic Wrist Design. *IEEE Trans. Robot.* **2019**, *35*, 261–277. [[CrossRef](#)]
10. Jiang, N.; Vest-Nielsen, J.L.; Muceli, S.; Farina, D. EMG-based simultaneous and proportional estimation of wrist/hand kinematics in uni-lateral trans-radial amputees. *J. Neuroeng. Rehabil.* **2012**, *9*, 42. [[CrossRef](#)] [[PubMed](#)]
11. Young, A.J.; Smith, L.H.; Rouse, E.J.; Hargrove, L.J. Classification of simultaneous movements using surface EMG pattern recognition. *IEEE Trans. Biomed. Eng.* **2012**, *60*, 1250–1258. [[CrossRef](#)] [[PubMed](#)]
12. Yatsenko, D.; McDonnall, D.; Guillory, K.S. Simultaneous, proportional, multi-axis prosthesis control using multichannel surface EMG. In Proceedings of the 2007 29th Annual International Conference of the IEEE Engineering in Medicine and Biology Society, Lyon, France, 22–26 August 2007; IEEE: Piscataway, NJ, USA, 2007; pp. 6133–6136.
13. Hahne, J.M.; Schweisfurth, M.A.; Koppe, M.; Farina, D. Simultaneous control of multiple functions of bionic hand prostheses: Performance and robustness in end users. *Sci. Robot.* **2018**, *3*, eaat3630. [[CrossRef](#)] [[PubMed](#)]
14. Ameri, A.; Akhaee, M.A.; Scheme, E.; Englehart, K. Real-time, simultaneous myoelectric control using a convolutional neural network. *PLoS ONE* **2018**, *13*, e0203835. [[CrossRef](#)] [[PubMed](#)]
15. Sartori, M.; Durandau, G.; Došen, S.; Farina, D. Robust simultaneous myoelectric control of multiple degrees of freedom in wrist-hand prostheses by real-time neuromusculoskeletal modeling. *J. Neural Eng.* **2018**, *15*, 066026. [[CrossRef](#)] [[PubMed](#)]
16. Engeberg, E. Biomimetic Controller for Increased Dexterity Prosthesis. U.S. Patent 10,543,111, 28 January 2020.
17. Blana, D.; Van Den Bogert, A.J.; Murray, W.M.; Ganguly, A.; Krasoulis, A.; Nazarpour, K.; Chadwick, E.K. Model-based control of individual finger movements for prosthetic hand function. *IEEE Trans. Neural Syst. Rehabil. Eng.* **2020**, *28*, 612–620. [[CrossRef](#)] [[PubMed](#)]
18. Al-Timemy, A.H.; Bugmann, G.; Escudero, J.; Outram, N. Classification of finger movements for the dexterous hand prosthesis control with surface electromyography. *IEEE J. Biomed. Health Inform.* **2013**, *17*, 608–618. [[CrossRef](#)] [[PubMed](#)]
19. Parajuli, N.; Sreenivasan, N.; Bifulco, P.; Cesarelli, M.; Savino, S.; Niola, V.; Esposito, D.; Hamilton, T.J.; Naik, G.R.; Gunawardana, U. Real-time EMG based pattern recognition control for hand prostheses: A review on existing methods, challenges and future implementation. *Sensors* **2019**, *19*, 4596. [[CrossRef](#)] [[PubMed](#)]
20. Antfolk, C.; D'Alonzo, M.; Controzzi, M.; Lundborg, G.; Rosen, B.; Sebelius, F.; Cipriani, C. Artificial redirection of sensation from prosthetic fingers to the phantom hand map on transradial amputees: Vibrotactile versus mechanotactile sensory feedback. *IEEE Trans. Neural Syst. Rehabil. Eng.* **2012**, *21*, 112–120. [[CrossRef](#)] [[PubMed](#)]
21. Kim, K.; Colgate, J.E. Haptic feedback enhances grip force control of sEMG-controlled prosthetic hands in targeted reinnervation amputees. *IEEE Trans. Neural Syst. Rehabil. Eng.* **2012**, *20*, 798–805. [[CrossRef](#)] [[PubMed](#)]
22. Meek, S.G.; Jacobsen, S.C.; Goulding, P.P. Extended physiologic taction: Design and evaluation of a proportional force feedback system. *J. Rehabil. Res. Dev.* **1989**, *26*, 53–62. [[PubMed](#)]
23. Chatterjee, A.; Chaubey, P.; Martin, J.; Thakor, N. Testing a prosthetic haptic feedback simulator with an interactive force matching task. *J. Prosthet. Orthot.* **2008**, *20*, 27–34. [[CrossRef](#)]
24. Ninu, A.; Dosen, S.; Muceli, S.; Rattay, F.; Dietl, H.; Farina, D. Closed-loop control of grasping with a myoelectric hand prosthesis: Which are the relevant feedback variables for force control? *IEEE Trans. Neural Syst. Rehabil. Eng.* **2014**, *22*, 1041–1052. [[CrossRef](#)] [[PubMed](#)]
25. Antfolk, C.; D'Alonzo, M.; Rosén, B.; Lundborg, G.; Sebelius, F.; Cipriani, C. Sensory feedback in upper limb prosthetics. *Expert Rev. Med. Devices* **2013**, *10*, 45–54. [[CrossRef](#)] [[PubMed](#)]
26. Štrbac, M.; Isaković, M.; Belić, M.; Popović, I.; Simanić, I.; Farina, D.; Keller, T.; Došen, S. Short-and long-term learning of feedforward control of a myoelectric prosthesis with sensory feedback by amputees. *IEEE Trans. Neural Syst. Rehabil. Eng.* **2017**, *25*, 2133–2145. [[CrossRef](#)] [[PubMed](#)]
27. Akhtar, A.; Sombeck, J.; Boyce, B.; Bretl, T. Controlling sensation intensity for electrotactile stimulation in human-machine interfaces. *Sci. Robot.* **2018**, *3*, eaap9770. [[CrossRef](#)] [[PubMed](#)]
28. Pacchierotti, C.; Sinclair, S.; Solazzi, M.; Frisoli, A.; Hayward, V.; Prattichizzo, D. Wearable haptic systems for the fingertip and the hand: Taxonomy, review, and perspectives. *IEEE Trans. Haptics* **2017**, *10*, 580–600. [[CrossRef](#)] [[PubMed](#)]
29. Stephens-Fripp, B.; Alici, G.; Mutlu, R. A review of non-invasive sensory feedback methods for transradial prosthetic hands. *IEEE Access* **2018**, *6*, 6878–6899. [[CrossRef](#)]
30. Pang, G.; Yang, G.; Pang, Z. Review of robot skin: A potential enabler for safe collaboration, immersive teleoperation, and affective interaction of future collaborative robots. *IEEE Trans. Med. Robot. Bionics* **2021**, *3*, 681–700. [[CrossRef](#)]
31. Cipriani, C.; Segil, J.L.; Clemente, F.; Edin, B. Humans can integrate feedback of discrete events in their sensorimotor control of a robotic hand. *Exp. Brain Res.* **2014**, *232*, 3421–3429. [[CrossRef](#)] [[PubMed](#)]

32. Aboseria, M.; Clemente, F.; Engels, L.F.; Cipriani, C. Discrete vibro-tactile feedback prevents object slippage in hand prostheses more intuitively than other modalities. *IEEE Trans. Neural Syst. Rehabil. Eng.* **2018**, *26*, 1577–1584. [[CrossRef](#)] [[PubMed](#)]
33. Mingrino, A.; Bucci, A.; Magni, R.; Dario, P. Slippage control in hand prostheses by sensing grasping forces and sliding motion. In Proceedings of the IEEE/RSJ International Conference on Intelligent Robots and Systems (IROS'94), Munich, Germany, 12–16 September 1994; IEEE: Piscataway, NJ, USA, 1994; pp. 1803–1809.
34. Romeo, R.A.; Zollo, L. Methods and sensors for slip detection in robotics: A survey. *IEEE Access* **2020**, *8*, 73027–73050. [[CrossRef](#)]
35. Kent, B.A.; Engeberg, E.D. Human-inspired feedback synergies for environmental interaction with a dexterous robotic hand. *Bioinspiration Biomim.* **2014**, *9*, 046008. [[CrossRef](#)] [[PubMed](#)]
36. Okamura, A.M.; Cutkosky, M.R. Feature detection for haptic exploration with robotic fingers. *Int. J. Robot. Res.* **2001**, *20*, 925–938. [[CrossRef](#)]
37. Fishel, J.A.; Loeb, G.E. Bayesian exploration for intelligent identification of textures. *Front. Neurobotics* **2012**, *6*, 4. [[CrossRef](#)] [[PubMed](#)]
38. Dahiya, R.S.; Metta, G.; Valle, M.; Sandini, G. Tactile sensing—From humans to humanoids. *IEEE Trans. Robot.* **2009**, *26*, 1–20. [[CrossRef](#)]
39. Alva, P.G.S.; Muceli, S.; Atashzar, S.F.; William, L.; Farina, D. Wearable multichannel haptic device for encoding proprioception in the upper limb. *J. Neural Eng.* **2020**, *17*, 056035. [[CrossRef](#)] [[PubMed](#)]
40. Abd, M.A.; Ingicco, J.; Hutchinson, D.T.; Tognoli, E.; Engeberg, E.D. Multichannel haptic feedback unlocks prosthetic hand dexterity. *Sci. Rep.* **2022**, *12*, 2323. [[CrossRef](#)] [[PubMed](#)]
41. Wolpert, D.M.; Goodbody, S.J.; Husain, M. Maintaining internal representations: The role of the human superior parietal lobe. *Nat. Neurosci.* **1998**, *1*, 529–533. [[CrossRef](#)] [[PubMed](#)]
42. Ades, C.; Abd, M.A.; Hutchinson, D.T.; Tognoli, E.; Du, E.; Wei, J.; Engeberg, E.D. Biohybrid Robotic Hand to Investigate Tactile Encoding and Sensorimotor Integration. *Biomimetics* **2024**, *9*, 78. [[CrossRef](#)] [[PubMed](#)]
43. Abd, M.A.; Bornstein, M.; Tognoli, E.; Engeberg, E.D. Armband with soft robotic actuators and vibrotactile stimulators for bimodal haptic feedback from a dexterous artificial hand. In Proceedings of the 2018 IEEE/ASME International Conference on Advanced Intelligent Mechatronics (AIM), Auckland, New Zealand, 9–12 July 2018; IEEE: Piscataway, NJ, USA, 2018; pp. 13–20.
44. Su, Z.; Hausman, K.; Chebotar, Y.; Molchanov, A.; Loeb, G.E.; Sukhatme, G.S.; Schaal, S. Force estimation and slip detection/classification for grip control using a biomimetic tactile sensor. In Proceedings of the 2015 IEEE-RAS 15th International Conference on Humanoid Robots (Humanoids), Seoul, Republic of Korea, 3–5 November 2015; IEEE: Piscataway, NJ, USA, 2015; pp. 297–303.
45. Choi, S.; Kuchenbecker, K.J. Vibrotactile display: Perception, technology, and applications. *Proc. IEEE* **2012**, *101*, 2093–2104. [[CrossRef](#)]
46. Islam, M.S.; Lim, S. Vibrotactile feedback in virtual motor learning: A systematic review. *Appl. Ergon.* **2022**, *101*, 103694. [[CrossRef](#)] [[PubMed](#)]
47. Engeberg, E.D.; Meek, S.G.; Minor, M.A. Hybrid force–velocity sliding mode control of a prosthetic hand. *IEEE Trans. Biomed. Eng.* **2008**, *55*, 1572–1581. [[CrossRef](#)] [[PubMed](#)]
48. Thomas, N.; Ung, G.; Ayaz, H.; Brown, J.D. Neurophysiological evaluation of haptic feedback for myoelectric prostheses. *IEEE Trans. Hum.-Mach. Syst.* **2021**, *51*, 253–264. [[CrossRef](#)]
49. Park, J.; Zahabi, M. Cognitive Workload Assessment of Prosthetic Devices: A Review of Literature and Meta-Analysis. *IEEE Trans. Hum.-Mach. Syst.* **2022**, *52*, 181–195. [[CrossRef](#)]
50. Kristoffersen, M.B.; Franzke, A.W.; Bongers, R.M.; Wand, M.; Murgia, A.; van der Sluis, C.K. User training for machine learning controlled upper limb prostheses: A serious game approach. *J. Neuroeng. Rehabil.* **2021**, *18*, 32. [[CrossRef](#)] [[PubMed](#)]
51. Simon, A.M.; Turner, K.L.; Miller, L.A.; Hargrove, L.J.; Kuiken, T.A. Pattern recognition and direct control home use of a multi-articulating hand prosthesis. In Proceedings of the 2019 IEEE 16th International Conference on Rehabilitation Robotics (ICORR), Toronto, ON, Canada, 24–28 June 2019; IEEE: Piscataway, NJ, USA, 2019; pp. 386–391.
52. Akhtar, A.; Cornman, J.; Austin, J.; Bala, D. Touch feedback and contact reflexes using the PSYONIC Ability Hand. In *MEC20 Symposium*; Psyonic, Inc.: San Diego, CA, USA, 2020.
53. Azeem, M.; Parveen, A. Study on Design and Performance Specifications of the Prosthetic Hands. In *Advancement in Materials, Manufacturing and Energy Engineering, Vol. I: Select Proceedings of ICAMME 2021*, Springer: Berlin/Heidelberg, Germany, 2022; pp. 119–135.
54. Abd, M.A.; Al-Saidi, M.; Lin, M.; Liddle, G.; Mondal, K.; Engeberg, E.D. Surface Feature Recognition and Grasped Object Slip Prevention with a Liquid Metal Tactile Sensor for a Prosthetic Hand. In Proceedings of the 2020 8th IEEE RAS/EMBS International Conference for Biomedical Robotics and Biomechatronics (BioRob), New York, NY, USA, 29 November–1 December 2020; IEEE: Piscataway, NJ, USA, 2020; pp. 1174–1179.
55. Zou, L.; Ge, C.; Wang, Z.J.; Cretu, E.; Li, X. Novel tactile sensor technology and smart tactile sensing systems: A review. *Sensors* **2017**, *17*, 2653. [[CrossRef](#)] [[PubMed](#)]
56. Capsi-Morales, P.; Piazza, C.; Catalano, M.G.; Grioli, G.; Schiavon, L.; Fiaschi, E.; Bicchi, A. Comparison between rigid and soft poly-articulated prosthetic hands in non-expert myo-electric users shows advantages of soft robotics. *Sci. Rep.* **2021**, *11*, 23952. [[CrossRef](#)] [[PubMed](#)]

57. Biddiss, E.A.; Chau, T.T. Upper limb prosthesis use and abandonment: A survey of the last 25 years. *Prosthet. Orthot. Int.* **2007**, *31*, 236–257. [[CrossRef](#)] [[PubMed](#)]
58. Smail, L.C.; Neal, C.; Wilkins, C.; Packham, T.L. Comfort and function remain key factors in upper limb prosthetic abandonment: Findings of a scoping review. *Disabil. Rehabil. Assist. Technol.* **2021**, *16*, 821–830. [[CrossRef](#)] [[PubMed](#)]
59. Yamada, H.; Yamanoi, Y.; Wakita, K.; Kato, R. Investigation of a cognitive strain on hand grasping induced by sensory feedback for myoelectric hand. In Proceedings of the 2016 IEEE International Conference on Robotics and Automation (ICRA), Stockholm, Sweden, 16–21 May 2016; IEEE: Piscataway, NJ, USA, 2016; pp. 3549–3554.
60. Shah, V.A.; Casadio, M.; Scheidt, R.A.; Mrotek, L.A. Spatial and temporal influences on discrimination of vibrotactile stimuli on the arm. *Exp. Brain Res.* **2019**, *237*, 2075–2086. [[CrossRef](#)] [[PubMed](#)]
61. Van Selst, M.; Ruthruff, E.; Johnston, J.C. Can practice eliminate the psychological refractory period effect? *J. Exp. Psychol. Hum. Percept. Perform.* **1999**, *25*, 1268. [[CrossRef](#)] [[PubMed](#)]
62. Pashler, H. Dual-task interference in simple tasks: Data and theory. *Psychol. Bull.* **1994**, *116*, 220. [[CrossRef](#)] [[PubMed](#)]
63. Wu, C.; Liu, Y. Queuing network modeling of the psychological refractory period (PRP). *Psychol. Rev.* **2008**, *115*, 913. [[CrossRef](#)] [[PubMed](#)]
64. Williams, S.R.; Okamura, A.M. Body-mounted vibrotactile stimuli: Simultaneous display of taps on the fingertips and forearm. *IEEE Trans. Haptics* **2020**, *14*, 432–444. [[CrossRef](#)] [[PubMed](#)]
65. Gescheider, G.A.; Wright, J.H.; Weber, B.J.; Kirchner, B.M.; Milligan, E.A. Reaction time as a function of the intensity and probability of occurrence of vibrotactile signals. *Percept. Psychophys.* **1969**, *5*, 18–20. [[CrossRef](#)]
66. Bao, T.; Su, L.; Kinnaird, C.; Kabeto, M.; Shull, P.B.; Sienko, K.H. Vibrotactile display design: Quantifying the importance of age and various factors on reaction times. *PLoS ONE* **2019**, *14*, e0219737. [[CrossRef](#)] [[PubMed](#)]
67. Jimenez, M.C.; Fishel, J.A. Evaluation of force, vibration and thermal tactile feedback in prosthetic limbs. In Proceedings of the 2014 IEEE Haptics Symposium (HAPTICS), Houston, TX, USA, 23–26 February 2014; IEEE: Piscataway, NJ, USA, 2014; pp. 437–441.
68. White, M.M.; Zhang, W.; Winslow, A.T.; Zahabi, M.; Zhang, F.; Huang, H.; Kaber, D.B. Usability comparison of conventional direct control versus pattern recognition control of transradial prostheses. *IEEE Trans. Hum.-Mach. Syst.* **2017**, *47*, 1146–1157. [[CrossRef](#)]
69. Krasoulis, A.; Vijayakumar, S.; Nazarpour, K. Multi-grip classification-based prosthesis control with two EMG-IMU sensors. *IEEE Trans. Neural Syst. Rehabil. Eng.* **2019**, *28*, 508–518. [[CrossRef](#)] [[PubMed](#)]
70. Cipriani, C.; Antfolk, C.; Controzzi, M.; Lundborg, G.; Rosén, B.; Carrozza, M.C.; Sebelius, F. Online myoelectric control of a dexterous hand prosthesis by transradial amputees. *IEEE Trans. Neural Syst. Rehabil. Eng.* **2011**, *19*, 260–270. [[CrossRef](#)]
71. Makin, T.R.; Filippini, N.; Duff, E.P.; Slater, D.H.; Tracey, I.; Johansen-Berg, H. Network-level reorganisation of functional connectivity following arm amputation. *Neuroimage* **2015**, *114*, 217–225. [[CrossRef](#)] [[PubMed](#)]
72. Hahamy, A.; Macdonald, S.N.; van den Heiligenberg, F.; Kieliba, P.; Emir, U.; Malach, R.; Johansen-Berg, H.; Brugger, P.; Culham, J.C.; Makin, T.R. Representation of multiple body parts in the missing-hand territory of congenital one-handers. *Curr. Biol.* **2017**, *27*, 1350–1355. [[CrossRef](#)] [[PubMed](#)]

Disclaimer/Publisher’s Note: The statements, opinions and data contained in all publications are solely those of the individual author(s) and contributor(s) and not of MDPI and/or the editor(s). MDPI and/or the editor(s) disclaim responsibility for any injury to people or property resulting from any ideas, methods, instructions or products referred to in the content.